Author(s): Achim, C. V. & Karttunen, M. & Elder, K. R. & Granato, E. & Ala-Nissilä, Tapio. & Ying, S. C.

Title: Phase diagram and commensurate-incommensurate transitions in the phase field crystal model with an external pinning potential

Year: 2006

Version: Final published version

Please cite the original version:

Achim, C. V. & Karttunen, M. & Elder, K. R. & Granato, E. & Ala-Nissilä, Tapio. & Ying, S. C. 2006. Phase diagram and commensurate-incommensurate transitions in the phase field crystal model with an external pinning potential. Physical Review E. Volume 74, Issue 2. P. 021104/1-8. ISSN 1539-3755 (printed). DOI: 10.1103/physreve.74.021104.

Phase diagram and commensurate-incommensurate transitions in the phase field crystal model with an external pinning potential

C. V. Achim
Laboratory of Physics, Helsinki University of Technology, P.O. Box 1100, FIN-02015 TKK, Finland

M. Karttunen
Department of Applied Mathematics, The University of Western Ontario, London, Ontario, Canada

K. R. Elder
Department of Physics, Oakland University, Rochester, Michigan 48309-4487, USA

E. Granato
Laboratório Associado de Sensores e Materiais, Instituto Nacional de Pesquisas Espaciais, São José dos Campos, São Paulo, Brazil

T. Ala-Nissila
Laboratory of Physics, Helsinki University of Technology, P.O. Box 1100, FIN-02015 TKK Helsinki, Finland and Department of Physics, Brown University, Providence, Rhode Island 02912-1843, USA

S. C. Ying
Department of Physics, Brown University, Providence, Rhode Island 02912-1843, USA
(Received 6 April 2006; published 4 August 2006)

We study the phase diagram and the commensurate-incommensurate transitions in a phase field model of a two-dimensional crystal lattice in the presence of an external pinning potential. The model allows for both elastic and plastic deformations and provides a continuum description of lattice systems, such as for adsorbed atomic layers or two-dimensional vortex lattices. Analytically, a mode expansion analysis is used to determine the ground states and the commensurate-incommensurate transitions in the model as a function of the strength of the pinning potential and the lattice mismatch parameter. Numerical minimization of the corresponding free energy shows reasonable agreement with the analytical predictions and provides details on the topological defects in the transition region. We find that for small mismatch the transition is of first order, and it remains so for the largest values of mismatch studied here. Our results are consistent with results of simulations for atomistic models of adsorbed overlayers.

DOI: 10.1103/PhysRevE.74.021104 PACS number(s): 64.60.Cn, 64.70.Rh, 68.43.De, 05.40.−a

I. INTRODUCTION

In nature there exist many modulated structures which possess two or more competing length scales. Such systems often exhibit commensurate-incommensurate (*C-I*) phase transitions [1,2], which are characterized by structural changes induced by competition between these different scales. Systems in this class that have received intense attention for many years include spin density waves [3,4] in Cr and charge-density wave systems [5], e.g., in "blue bronze." They are characterized by an order parameter (e.g., charge or spin density) that is modulated in space with a given wave vector q. In these systems the transition from a commensurate (C) state to an incommensurate (I) state is controlled by temperature and interaction with defects of the lattice [6]. Other systems of interest are materials that exhibit magnetic phase with spiral-like structures [7,8]. Finally, vortex lattices in superconducting films with pinning centers [9] and weakly adsorbed monolayers [10,11] on a substrate comprise a two-dimensional (2D) realization of systems exhibiting *C-I* transitions. In these systems, the interparticle interactions are minimized by a configuration with a lattice constant a, while the substrate-adsorbed monolayer interaction is minimized by a configuration with lattice constant b, usually incommensurate with a.

The simplest theoretical model for a *C-I* transition is the one-dimensional (1D) Frenkel-Kontorova (FK) model [12,13]. It consists of a chain of particles interconnected by springs, representing an adsorbate layer, and placed in a periodic potential describing the effects of a substrate. The potential energy of such a system is given by

$$U = \sum_n \left[\frac{\lambda}{2}(x_{n+1} - x_n - a)^2 + V(x_n) \right], \tag{1}$$

where a is the equilibrium lattice spacing of the chain in the absence of a potential and λ is the stiffness. The potential function $V(x_n)$ has periodicity b and can be approximated by a cosine function

$$V(x_n) = V_0 \left[1 - \cos\left(\frac{2\pi x_n}{b} \right) \right]. \tag{2}$$

When V_0 is sufficiently small, the adsorbate lattice will be independent of the potential. This structure is called a "floating" phase and the lattice spacing $\tilde{a} = \lim_{x\to\infty}(x_n - x_0)/n$ of the adsorbate lattice can be an arbitrary multiple of the substrate

periodicity. In general, the floating phase is incommensurate for almost all values of the ratio $\tilde{a}/b$.

In the opposite limit, when the potential is very strong, one can expect the lattice to relax into a commensurate structure where the average lattice spacing of the adsorbed atoms is a simple rational fraction of the period b. In the I phase, close to the C-I transition, it is energetically more favorable for the system to form C regions separated by domain walls in which the springs are stretched or compressed and the commensurate registry with the potential is lost. These domain walls are usually called discommensurations and the corresponding region in the phase diagram within the I phase will be referred to as a modulated (M) phase. A positive (negative) discommensuration leads to a reduction (increase) in the density of adsorbate atoms and these regions are referred to as light (heavy) walls.

The C-I transition can be determined by examining the behavior of the winding number $\tilde{\Omega}=\tilde{a}/b$ as a function of $\Omega=a/b$ for fixed V_0. If V_0 is larger than a certain critical value V_c, the system will be commensurate for all the values of Ω. The function $\tilde{\Omega}(\Omega)$ has a staircase type of appearance, and thus, for $V_0<V_c$ it is called an incomplete devil's staircase, and for $V_0>V_c$, a complete devil's staircase [2,14]. If there are discontinuities or first order jumps between commensurate states, it is called a harmless staircase [15]. In the continuum version of the FK model, where there are no devil's staircase [15], the C-I transition is second order with a correlation length, identified as the domain wall separation, which diverges logarithmically near the transition.

The FK model can be extended to two dimensions to describe, for example, adsorbed layers on crystal surfaces. In its simplest version, the 2D FK model [2] describes the adsorbate interactions by a pure harmonic potential in a periodic pinning potential. Although the FK model takes into account topological defects in the form of domain walls, it leaves out plastic deformations of the layer due to topological defects such as dislocations. These defects are particularly important when the CI transition occurs between two different crystal structures or in the presence of temperature fluctuations or quenched disorder.

They are automatically included in a full microscopic model involving interacting atoms in the presence of a substrate potential. However, the full complexities of the microscopic model limits the actual numerical computation to systems of relatively small sizes. The size effect could be very strong for CI transition involving extended domains or topological defects. Recently, a phase field crystal model was introduced [16,17] that allows for both elastic and plastic deformations in the solid phase. In this formulation a free energy functional is introduced, which depends on a density averaged over microscopic times scales, $\Phi(\vec{r},t)$. The free energy is minimized when Φ is spatially periodic (i.e., crystalline) in the solid phase and constant in the liquid phase. By incorporating phenomena on atomic length scales, the approach naturally includes elastic and plastic deformations, multiple crystal orientations, and anisotropic structures, in a manner similar to other microscopic approaches such as molecular dynamics. However, the phase field crystal (PFC) method describes the density on a diffusive and not the real microscopic times scales. It is therefore computationally much more efficient. Thus, this model should provide a suitable description of the C-I transition when topological defects, domain walls, and dislocations are present.

In this work, we extend the 2D PFC model [16,17] to include the influence of an external pinning potential. Such a model should provide a suitable continuum description of lattice systems such as weakly adsorbed atomic overlayers or 2D vortex lattices with pinning. The pinning potential is chosen such that it induces C-I transitions between ground states of different symmetries in the model. The outline of the paper is as follows. We first define the model and carry out an analytic mode expansion to determine the crystal structure and the location of the C-I transition lines. We analyze these transitions as a function of the lattice mismatch and strength of the potential. Following this we carry out a numerical minimization of the full free energy functional, which gives reasonable agreement with the theoretical predictions and provides details on the nature of the topological defects near the transition. Finally, we discuss the nature of the C-I transitions and the relation of our results to atomistic simulations for adsorbed overlayers [18].

II. THE PHASE FIELD CRYSTAL MODEL

In the PFC model [16,17], the free energy functional is written as

$$\mathcal{F}=\int d\vec{r}\left[\frac{a\Delta T}{2}\Phi^2+u\frac{\Phi^4}{4}+\frac{\Phi}{2}G(\nabla^2)\Phi\right], \tag{3}$$

where $G(\nabla^2)=\lambda(q_0^2+\nabla^2)^2$, and its eigenvalues can be related to the experimental structure factor of, e.g., Ar [17]. Equation (3) describes a crystal with a lattice constant of $2\pi/q_0$, while the elastic properties can be adjusted by λ, u, and q_0. For numerical calculation it is convenient to rewrite the free energy in dimensionless units [16,17] as

$$\vec{x}=\vec{r}q_0,\quad \psi=\Phi\sqrt{\frac{u}{\lambda q_0^4}},\quad r=\frac{a\Delta T}{\lambda q_0^4},\quad \tau=\Gamma\lambda q_0^4 t. \tag{4}$$

In these units the free energy becomes

$$F=\frac{\mathcal{F}}{\lambda^2 q^{8-d}/u}=\int d\vec{x}\left[\frac{\psi}{2}\omega(\nabla^2)\psi+\frac{\psi^4}{4}\right], \tag{5}$$

where $\omega\ (\nabla^2)=r+(1+\nabla^2)^2$. Since ψ is a conserved field, it satisfies the following equation of motion:

$$\frac{\partial\psi}{\partial\tau}=\nabla^2\frac{\delta F}{\delta\psi}+\zeta=\nabla^2[\omega(\nabla^2)\psi+\psi^3]+\zeta, \tag{6}$$

where ζ has zero mean, $\langle\zeta(\vec{x}_1,\tau_1)\zeta(\vec{x}_2,\tau_2)\rangle=\mathcal{D}\nabla^2\delta(\vec{x}_1-\vec{x}_2)\delta(\tau_1-\tau_2)$, and $\mathcal{D}$ is a constant. Equations (5) and (6) have been used to study a variety of phenomena involving elastic and plastic deformation including grain boundary energies between misaligned grains, buckling and dislocation nucleation in liquid phase epitaxial growth, the reverse Hall-Petch effect in nanocrystalline materials, grain growth, and ductile fracture [17].

In 2D the free energy in Eq. (5) in the absence of external potential is minimized by three distinct solutions for the di-

mensionless field ψ; constant, stripes, and dots. For the purposes of this work, only the latter solution is relevant. This solution consists of a triangular distribution of density maxima corresponding to a crystalline phase. In general, this solution can be written as

$$\psi(\vec{r}) = \sum_{n,m} a_{n,m} e^{i\vec{G}_{nm}\vec{r}} + \bar{\psi}, \tag{7}$$

where $\vec{G}_{nm} \equiv n\vec{b}_1 + m\vec{b}_2$, $\vec{b}_1$ and $\vec{b}_2$ are the reciprocal lattice vectors, and $\bar{\psi}$ is the average value of ψ. For a triangular lattice, $\vec{b}_1$ and $\vec{b}_2$ can be written as

$$\vec{b}_1 = \frac{2\pi}{a_t\sqrt{3}/2}(\sqrt{3}/2\hat{x} + \hat{y}/2),$$

$$\vec{b}_2 = \frac{2\pi}{a_t\sqrt{3}/2}\hat{y}, \tag{8}$$

where a_t is the distance between nearest-neighbor (local) maxima of ψ (corresponding to the "atomic" positions). The amplitudes $a_{m,n}$ and lattice spacing a_t are determined by minimizing the free energy functional. For simplicity, it is useful to first consider a simple one-mode approximation in which only pairs (n,m) that correspond to $|\vec{G}_{n,m}| = 2\pi/(a_t\sqrt{3}/2)$ are retained. In this limit ψ can be written

$$\psi_t = A_t[\cos(q_t x)\cos(q_t y/\sqrt{3}) - \cos(2q_t y/\sqrt{3})/2] + \bar{\psi}, \tag{9}$$

where A_t is an unknown constant and $q_t = 2\pi/a_t$. Substituting Eq. (9) in Eq. (5) and minimizing with respect to A_t and q_t gives, $A_t = 4[\bar{\psi} + (-15r - 36\bar{\psi}^2)^{1/2}/3]/5$, $q_t = \sqrt{3}/2$, and

$$F^t_{min}/S = -\frac{1}{10}\left(r^2 + \frac{13}{50}\bar{\psi}^4\right) + \frac{\bar{\psi}^2}{2}\left(1 + \frac{7}{25}r\right) + \frac{4\bar{\psi}}{25}\sqrt{-15r - 36\bar{\psi}^2}\left(\frac{4\bar{\psi}^2}{5} + \frac{5}{3}\right). \tag{10}$$

As shown in Ref. [17], this approximation is valid in the limit of small r. In the next section, an external pinning potential with square symmetry will be introduced in the PFC model. As will be shown, depending on the strength of the external potential and the lattice mismatch, a commensurate-incommensurate transition would occur.

III. PHASE DIAGRAM WITH EXTERNAL POTENTIAL

In the PFC model, an external potential V is introduced by adding a term coupling V linear to ψ in the free energy functional given in Eq. (5), i.e.,

$$F = \int d\vec{x}\left[\frac{\psi}{2}\omega(\nabla^2)\psi + \frac{\psi^4}{4} + \psi V\right]. \tag{11}$$

In this study, we consider an external potential of square symmetry, which is distinct from the symmetry of the triangular lattice in the absence of the external potential [e.g, Eq. (9)].

$$V = V_0\cos(q_s x)\cos(q_s y), \tag{12}$$

where $q_s = 2\pi/(a_s\sqrt{2})$. We define the relative mismatch δ_m between the external potential and adsorbed monolayer as

$$\delta_m = 1 - 2\pi/a_s. \tag{13}$$

With the above external potential, the PFC model corresponds to a continuous description of *C-I* transitions and could describe, for example, an adsorbed layer on the (100) face of an fcc crystal [18].

To understand the influence of V on the minimum energy solution, we can again Fourier analyze the equilibrium density. Taking into account both the intrinsic triangular symmetry and the external potential of square symmetry, the system is best described by a combination of hexagonal and square modes. In this case the corresponding hexagonal-square mode approximation (HSMA) can be written as

$$\psi_{HMSA} = A_1\cos(q_s x)\cos(q_s y) + A_2[\cos(2q_s x) + \cos(2q_s y)] + A_t[\cos(q_t x)\cos(q_t y/\sqrt{3}) - \cos(2q_t y/\sqrt{3})/2] + \bar{\psi}. \tag{14}$$

This Fourier expansion includes the basic mode for the triangular lattice as done in Eq. (9) and the first two harmonics for the commensurate modes with square symmetry. In general, they describe an incommensurate phase corresponding to a triangular phase distorted by the square symmetry external potential. However, when the mismatch is sufficiently large and/or the strength of the external potential is sufficiently strong, the solution that minimizes the free energy will correspond to a vanishing value for A_t and a commensurate phase.

The free-energy density in the HSMA is given by

$$F^{HSMA}/S = \frac{9}{256}A_1^4 + \frac{9}{16}A_2^4 + A_1^2\left(\frac{1}{8} + \frac{r}{8} + \frac{3\bar{\psi}^2}{8} - \frac{1}{2}q_s^2 + \frac{1}{2}q_s^4\right) + A_2^2\left(\frac{1}{2} + \frac{3}{2}\bar{\psi}^2 + r\frac{1}{2} + 8q_s^4 - 4q_s^2\right) + \frac{9}{16}A_t^2\left(\frac{1}{4}A_1^2 + A_2^2\right) + A_1^2\left(\frac{9}{16}A_2^2 + \frac{3}{4}A_2\bar{\psi}\right) + \frac{V_0 A_1}{4} + F^t/S. \tag{15}$$

The coefficients A_t, A_1, and A_2 are unknown and must be chosen to minimize the free-energy density.

The analytic expressions for the free energies can now be used to obtain the phase diagram of the pinned PFC model as a function of the pinning strength V_0 and the mismatch δ_m. To this end Eq. (15) can be used to determine the critical value of V_0, V_c, at which the *C-I* transition occurs, identified by the point where the amplitude of the triangular phase vanishes, i.e., when $A_t(V_0, \delta_m) = 0$. The results are shown in Fig. 1(a). Within the HSMA, the *C-I* transitions are discontinuous and become continuous only for infinite δ_m. In the next section we will compare the analytically obtained phase diagram in the HSMA approximation with a full numerical minimization of the total free energy.

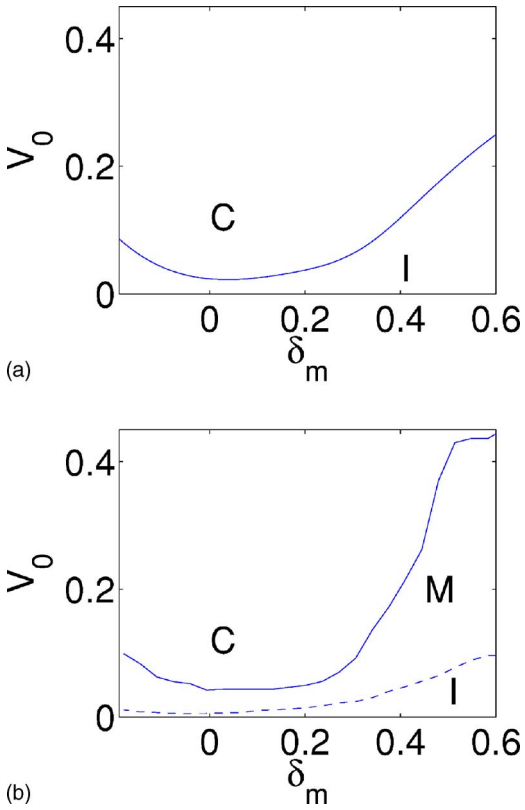

FIG. 1. (Color online) (a) The phase diagram calculated analytically using the HSMA approximation for the free energy. The region denoted by *C* is the commensurate phase and *I* denotes the incommensurate phase. (b) The corresponding phase diagram determined numerically, as explained in Sec. IV. The dashed line corresponds to a crossover regime between the fully incommensurate *I* and the modulated *M* phases. See the text for details.

IV. NUMERICAL RESULTS

A. Energy minimization

While the HSMA yields a good qualitative understanding for the phase diagram describing the CI transition, it is not quantitatively accurate, particularly near the transition, since the HSMA cannot describe the structure of the domain walls and other possible topological defects. In this section, we describe the full numerical investigation of the *C-I* transition in the PFC model. This is obtained by direct minimization of the free-energy functional without any assumed form for the density field.

In the presence of the external potential, the equation of motion for ψ becomes

$$\frac{\partial \psi}{\partial \tau} = \nabla^2[\omega(\nabla^2)\psi + \psi^3 + V] + \zeta. \tag{16}$$

The minimal energy numerical solutions for the equilibrium states of ψ were obtained by solving $\delta F/\delta\psi = 0$ using a simple relaxational method similar to the usual molecular dynamics annealing scheme. The noise term ζ in Eq. (16) is only used as an annealing tool to escape from any metastable states. It is applied for a limited period of time only and then set back to zero. For the remainder of the time, Eq. (16) was solved using a simple Euler algorithm, i.e.,

$$\psi_{n+1,i,j} = \psi_{n,i,j} + \Delta\tau\nabla^2(\{[r + (1 + \nabla^2)^2]\psi_{n,i,j} + \psi^3_{n,i,j} + V_{n,i,j}\}), \tag{17}$$

where the Laplacian operator ∇^2 represents the lattice second-order derivatives. A so-called spherical Laplacian approximation [17] was used for ∇^2. For a thorough discussion on solving differential equations numerically using stencils, see Ref. [19].

Equation (17) was solved on a 512×512 grid with the spatial discretization $dx = 1$ and time step $\Delta\tau = 0.02$ using periodic boundary conditions. The parameters r and $\bar{\psi}$ were chosen to correspond to a crystalline region of phase space, i.e., $r = -1/4$ and $\bar{\psi} = -1/4$. However, a hexagonal lattice cannot be fitted in a square geometry and in order to satisfy the periodic boundary conditions, the lattice will be distorted and it may exhibit domains of different orientations separated by walls, thereby giving a free-energy density higher than that of the ground state. The value of dx also influences the free-energy density when lattice constant is small. We have checked the finite-size effects for our lattice in the absence of pinning potential, the relative difference between free-energy density F^n/S and the one-mode approximation is only about 0.56%.

B. Phase diagram and ground state configurations

The free-energy density and the structure factor $S(|\vec{k}|) = S(k) = |\tilde{\psi}(|\vec{k}|)|^2$ were calculated numerically for several different values of $2\pi/a_s$ as allowed by the periodic boundary conditions. In Fig. 2, a set of configurations for the model with increasing amplitude of the pinning potential V_0 are shown. As expected, for $V_0 = 0$ the ground state has perfect triangular symmetry. With increasing amplitude of the square pinning potential, the configurations become spatially distorted and eventually the system undergoes a transition to a square lattice.

We define the position of the *C-I* transition by analyzing the structure factor $S(k)$. The transition occurs when the peaks of the structure factor that correspond to the square lattice begin to split as shown in Figs. 3 and 4.

Next, the approximate analytic solutions for the free energy are compared to the numerical ones as a function of pinning potential for fixed mismatch. As seen in Fig. 5, the free-energy density decreases as a function of the pinning strength. For small values of δ_m, the transition to square symmetry occurs at relatively weak pinning strengths and is first order. For larger values of δ_m, the free energy decreases slowly and the *C-I* transition appears continuous [see Fig. 5(a)]. However, we have checked the finite-size dependence up to systems of linear size 1024 and find that for up to at least $\delta_m = 0.52$, the transition remains first order. We note that a first-order CI transition is in fact consistent with theoretical predictions based on models of interacting domain walls on a

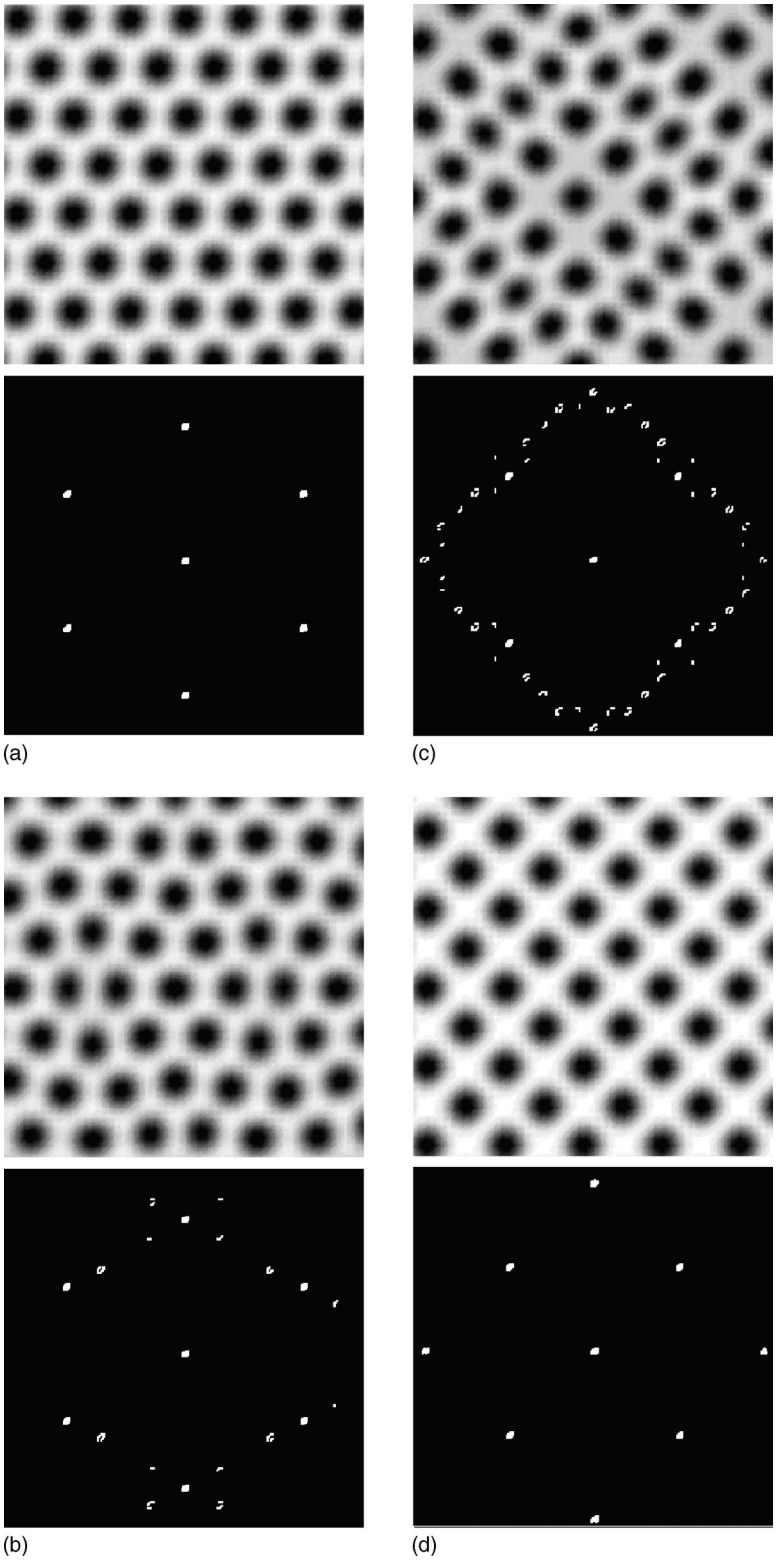

FIG. 2. Snapshots of ground states and the corresponding structure factors (lower figures) showing the transition of the system from a triangular lattice for zero pinning to a square lattice for $\delta_m=0.14$ (only a small part of the lattice is shown here).

pinning potential with square symmetry [20]. In Fig. 5 we can also see that the analytical HSMA gives reasonable agreement with the numerical results, especially for large misfit where domain structures are not as predominant.

Finally, we determined the onset of the modulated (M) phase within the I phase by the value of V_0 where the peaks in the structure factor corresponding to the triangular symmetry split in multiple peaks. In the present model the M phase corresponds to regions commensurate with the pinning potential, but separated by heavy domain walls of excess of local density (see also Fig. 7). The dashed lines indicate the threshold value where domain walls appear in the system, shown in Figs. 1 and 5(a)–5(c) (in the insets) by dashed lines.

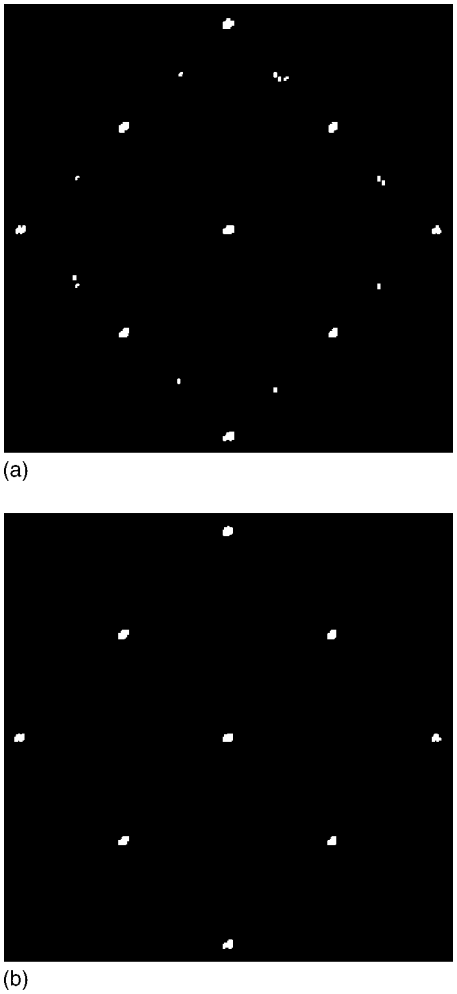

FIG. 3. Splitting of the peaks of the structure factor with decreasing pinning potential in the vicinity of the *C-I* transition for $\delta_m=0.14$. The splitting is discontinuous, suggesting a first-order-like transition.

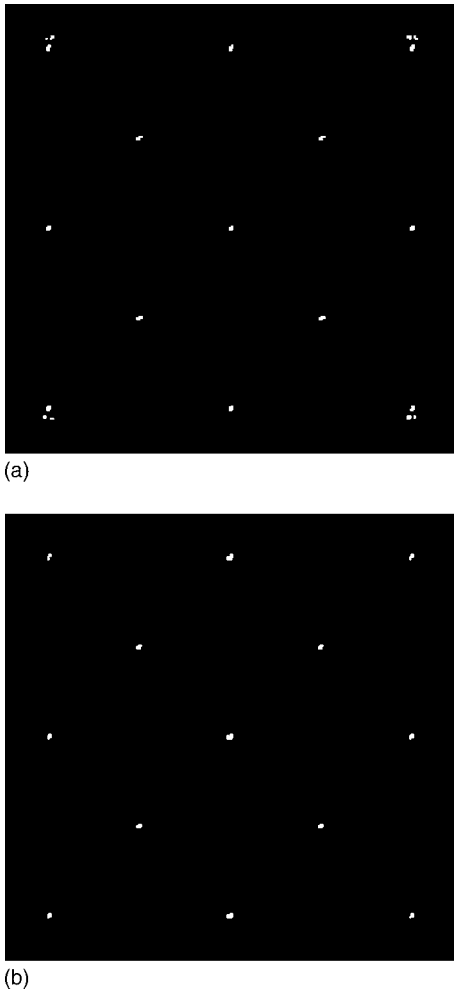

FIG. 4. Splitting of the peaks of the structure factor with decreasing pinning potential in the vicinity of the *C-I* transition for $\delta_m=0.52$. The splitting is much smaller than in Fig. 3 but remains discontinuous. See the text for details.

C. Voronoi analysis of domain walls

It is of further interest to analyze the nature of the spatial configurations and domain walls in the *I* phase and in the transition region. A convenient way to quantify the defects is to use the Voronoi analysis [21,22]. By definition, the Voronoi cell of any particle contains all the points that are closer to it than any other particle, i.e., it defines the Wigner-Seitz cell for each particle. The resulting cells are polygons with *N* sides that represents the number of nearest neighbors (NNs). In the present case, this is particularly useful since very close to the transition region there is some variation in the positions and sizes of the density maxima, identified as effective "particles" in our phase field crystal model. In Fig. 6 we show the results of Voronoi analysis of our data as a function of the pinning strength for a fixed mismatch $\delta_m=0.14$. For weak pinning, Voronoi cells with $N=6$ dominate as expected. Closer to the CI transition line (shown with a vertical line), contributions from $N=5$ become important and in the immediate vicinity of the CI transition virtually all Voronoi cells have $N=4$. The Voronoi cell analysis can be used to identify the location and nature of the domain walls. Close to the CI transition, the system is composed of regions commensurate with the pinning potential but separated by heavy walls. These configurations appear spontaneously and have been observed also in Monte Carlo simulations of overlayers of atoms interacting via the Lennard-Jones potential adsorbed on the (100) face of a fcc crystal [18]. In Fig. 7 we show results for the present model in the corresponding region. The density of maxima is smoothed with a Gaussian function with a width of approximately $3a_s$. As can be seen in Fig. 7(a), the system indeed comprises commensurate regions separated by walls. The regions of high density indicate "heavy" domain walls with an excess of particles compared to the commensurate regions. In these regions the particles are plotted with black circles while in the commensurate regions white circles are used. In Fig. 7(b) we show the contribution of different Voronoi polygons in this state. The fraction of polygons with $N=5$ (p_5) is 0.53, while the fraction with $N=4$ (p_4) and $N=6$ (p_6) are 0.16 and 0.29, respectively, which agrees well with results in Ref. [18].

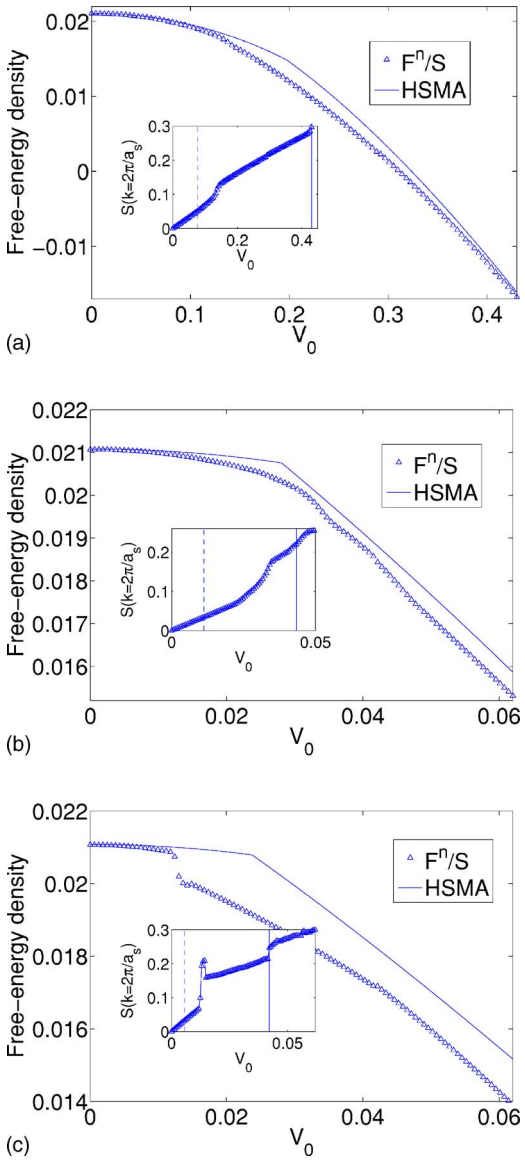

FIG. 5. (Color online) Comparison of the free-energy densities between analytical (HSMA) and numerical results for different values of δ_m. The inset represents intensity of the peaks of the structure factor corresponding to the reciprocal vectors of magnitude $k=2\pi/a_s$. The continuous vertical lines represent the position of the *C-I* transition, while the dashed lines mark the crossover regime in the *I* phase.

V. DISCUSSION AND CONCLUSIONS

In this work we have considered the recently developed crystal phase field model [17] in the presence of an external pinning potential. As the model naturally incorporates both elastic and plastic deformations, it provides a continuum description of lattice systems such as adsorbed atomic layers or 2D vortex lattices, while still retaining the discrete lattice symmetry of the solid phase. The main advantage of the model as compared to traditional approaches is that despite retaining spatial resolution on an atomic scale, its temporal evolution naturally follows diffusive time scales. Thus, the numerical simulations studies of the dynamics of the systems

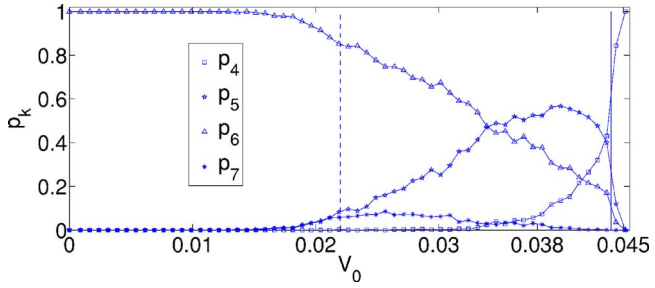

FIG. 6. (Color online) Relative contributions of the Voronoi polygons with k NNs (p_k, $k=4,5,6,7$) as a function of the pinning strength, with $\delta_m=0.14$. The continuous line represents the *C-I* transition, while the dashed line marks the crossover regime within the *I* phase.

such as approach to equilibrium can be achieved over realistic time scales many order of magnitudes over the microscopic atomic models. We have taken advantage of this and considered the full phase diagram of the model as a function

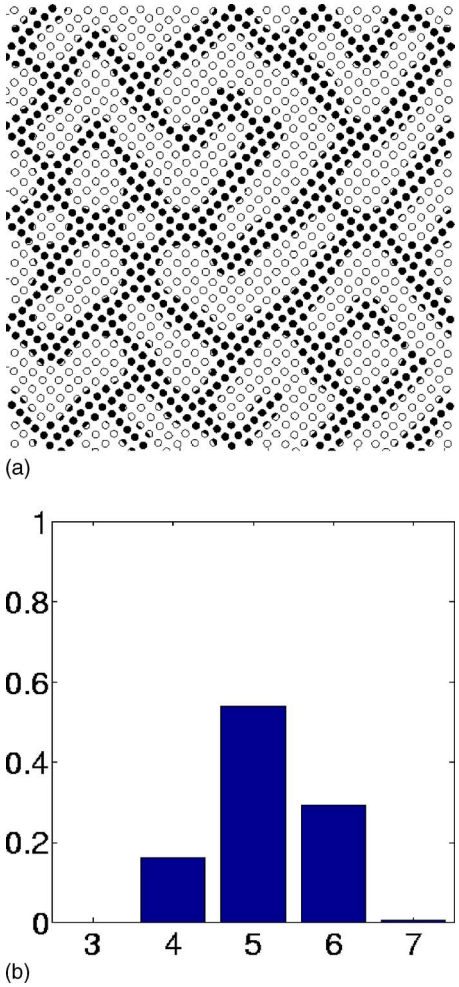

FIG. 7. (Color online) (a) Example of modulated phase obtained from the system characterized by $\delta_m=0.14$, $V_0=0.043$. The dark areas represent the *I* regions, i.e., heavy walls, while the light areas are *C* regions. The positions of the particles are superimposed on the density maxima. (b) The contribution of Voronoi polygons in this state. See the text for details.

of the lattice mismatch and pinning strength, both analytically and numerically. A systematic mode expansion analysis has been used to determine the ground states and the commensurate-incommensurate transitions in the model. Numerical minimization of the corresponding free energy shows reasonable agreement with the analytical predictions and provides details on the topological defects in the transition region. In particular, we find that the transition remains discontinuous for all values of the mismatch studied here. We have also performed a detailed Voronoi analysis of the domain walls throughout the transition region. Our results are consistent with simulations for atomistic models of pinned overlayers on surfaces.

A particularly interesting application of the present model is to pinned systems that are driven by external force. Examples of such systems include driven adsorbed monolayers [23], driven charge density waves [24], and driven flux lattices [25]. Work in these problems is already in progress.

ACKNOWLEDGMENTS

This work has been supported in part by the Academy of Finland through its Center of Excellence grant for the COMP CoE. M.K. has been supported by NSERC of Canada. E.G. has been supported by Fundação de Amparo à Pesquisa do Estado de São Paulo-FAPESP (Grant No. 03/00541-0). K.R.E. acknowledges support from the National Science Foundation under Grant No. DMR-0413062.

[1] M. Schick, Prog. Surf. Sci. **11**, 245 (1981).
[2] P. Bak, Rep. Prog. Phys. **45**, 587 (1982).
[3] P. F. Tua and J. Ruvalds, Phys. Rev. B **32**, 4660 (1985).
[4] E. Fawcett, Rev. Mod. Phys. **60**, 209 (1988).
[5] R. M. Fleming, L. F. Schneemeyer, and D. E. Moncton, Phys. Rev. B **31**, 899 (1985).
[6] W. L. McMillan, Phys. Rev. B **12**, 1187 (1975).
[7] A. Zheludev, S. Maslov, G. Shirane, Y. Sasago, N. Koide, and K. Uchinokura, Phys. Rev. Lett. **78**, 4857 (1997).
[8] I. E. Dzyaloshinskii, Sov. Phys. JETP **20**, 665 (1965).
[9] J. I. Martín, M. Vélez, J. Nogués, and Ivan K. Schuller, Phys. Rev. Lett., **79**, 1929 (1997).
[10] A. Thomy, X. Duval, and J. Regnier, Surf. Sci. Rep. **1**, 1 (1980).
[11] R. Pandit, M. Schick, and M. Wortis, Phys. Rev. B **26**, 5112 (1982).
[12] T. A. Kontorova and Y. I. Frenkel, Zh. Eksp. Teor. Fiz. **8**, 89 (1939).
[13] P. M. Chaikin and T. C. Lubensky, *Principles of Condensed Matter Physics* (Cambridge University Press, New York, 1995).
[14] M. H. Jensen, P. Bak, and T. Bohr, Phys. Rev. Lett. **50**, 1637 (1983).
[15] J. Villain and M. B. Gordon, J. Phys. C, **13**, 3117 (1980), M. E. Fisher and W. Selke, Phys. Rev. Lett. **44**, 1502 (1980).
[16] K. R. Elder, M. Katakowski, M. Haataja, and M. Grant, Phys. Rev. Lett. **88**, 245701 (2002).
[17] K. R. Elder and M. Grant, Phys. Rev. E **70**, 051605 (2004).
[18] A. Patrykiejew, S. Sokolowski, and K. Binder, J. Chem. Phys. **115**, 983 (2001).
[19] M. Patra and M. Karttunen, Numer. Methods Partial Differ. Equ. (to be published).
[20] F. S. Rys, Phys. Rev. Lett. **51**, 849 (1983).
[21] W. Shinoda and S. Okazaki, J. Chem. Phys. **109**, 1517 (1998).
[22] E. G. Flekkoy, P. V. Coveney, and G. De Fabritiis, Phys. Rev. E **62**, 2140 (2000).
[23] Gang He and Mark O. Robbins, Phys. Rev. B **64**, 035413 (2001).
[24] C. R. Myers and J. P. Sethna, Phys. Rev. B **47**, 11171 (1993).
[25] C. J. Olson, C. Reichhardt, and Franco Nori, Phys. Rev. Lett. **81**, 3757 (1998).